Heat wave frequency variability over North America: Two distinct leading modes

Zhiwei Wu,[1] Hai Lin,[1] Jianping Li,[2] Zhihong Jiang,[3] and Tingting Ma[3]

Received 21 September 2011; revised 11 November 2011; accepted 11 November 2011; published 18 January 2012.

[1] Seasonal prediction of heat wave variability is a scientific challenge and of practical importance. This study investigates the heat wave frequency (HWF) variability over North America (NA) during the past 53 summers (1958–2010). It is found that the NA HWF is dominated by two distinct modes: the interdecadal (ID) mode and the interannual (IA) mode. The ID mode primarily depicts a HWF increasing pattern over most of the NA continent except some western coastal areas. The IA mode resembles a tripole HWF anomaly pattern with three centers over the northwestern, central, and southern NA. The two leading modes have different dynamic structures and predictability sources. The ID mode is closely associated with the prior spring sea surface temperature anomaly (SSTA) in the tropical Atlantic and tropical western Pacific that can persist throughout the summer, whereas the IA mode is linked to the development of El Niño–Southern Oscillation. A simplified general circulation model is utilized to examine the possible physical mechanism. For the ID mode the tropical Atlantic SSTA can induce a Gill-type response which extends to NA, while the northwestern Pacific SSTA excites a Rossby wave train propagating eastward toward NA. These two flow patterns jointly contribute to the formation of the large-scale circulation anomalies associated with the ID mode. For the IA mode the corresponding circulation anomalies are basically similar to a Pacific-North America pattern. The subsidence associated with high-pressure anomalies warms and dries the boundary layer, inhibiting cloud formation. The resulting surface radiative heating further warms the surface. For the low-pressure anomalies the situation is just opposite. Through such processes these SSTAs can exert profound influences on the HWF variability over NA.

Citation: Wu, Z., H. Lin, J. Li, Z. Jiang, and T. Ma (2012), Heat wave frequency variability over North America: Two distinct leading modes, *J. Geophys. Res.*, *117*, D02102, doi:10.1029/2011JD016908.

1. Introduction

[2] Extreme weather and climate events, such as heat waves, have received increased attention during the past decade owing to the often large loss of human life and exponentially increasing costs associated with them [*Karl and Easterling*, 1999; *Easterling et al.*, 2000; *Trenberth et al.*, 2007]. For instance, in the summer of 2003, heat waves resulted in more than 25,000 deaths in Europe [*Garcia-Herrera et al.*, 2010]. In 2010 summer, Moscow experienced 33 consecutive days with maximum temperatures exceeding 30 °C [*Alexander*, 2010]. In the past decades, northern China has been undergoing frequent heat waves which amplify the local droughts and desertification, more than half a billion people being facing drinking water shortages [e.g., *Wang and Ding*, 2006; *Ding et al.*, 2007]. Under such a background, investigation on heat wave variability becomes an urgent issue, globally.

[3] Heat wave anomalies often exhibit notable place-to-place differences. Although heat waves would become more intense, longer lasting, and/or more frequent in a warmer climate with increased mean temperatures [e.g., *Karl and Trenberth*, 2003], such changes are not evenly distributed in space but are characterized instead by particular patterns related to the larger-scale climate change [e.g., *Meehl et al.*, 2004]. *Meehl and Tebaldi* [2004] found that heat waves over North America (NA) in the 21st century may exhibit a distinct geographic pattern change based on a global coupled climate model projection. In spite that the heat wave variability may be related to changes in the local drought and wet spells [e.g., *Dai et al.*, 1998], it is, however, still not clear what kind of modes dominate heat waves over NA during the past decades.

[4] Predicting heating waves is probably another challenging issue. Owing to the chaotic nature of the atmospheric motion, the detailed evolution of heat waves is unpredictable

[1]Meteorological Research Division, Environment Canada, Dorval, Quebec, Canada.
[2]State Key Laboratory of Numerical Modeling for Atmospheric Sciences and Geophysical Fluid Dynamics, Institute of Atmospheric Physics, Chinese Academy of Sciences, Beijing, China.
[3]Key Laboratory of Meteorological Disaster of Ministry of Education, University of Information Science and Technology, Nanjing, China.

0148-0227/12/2011JD016908

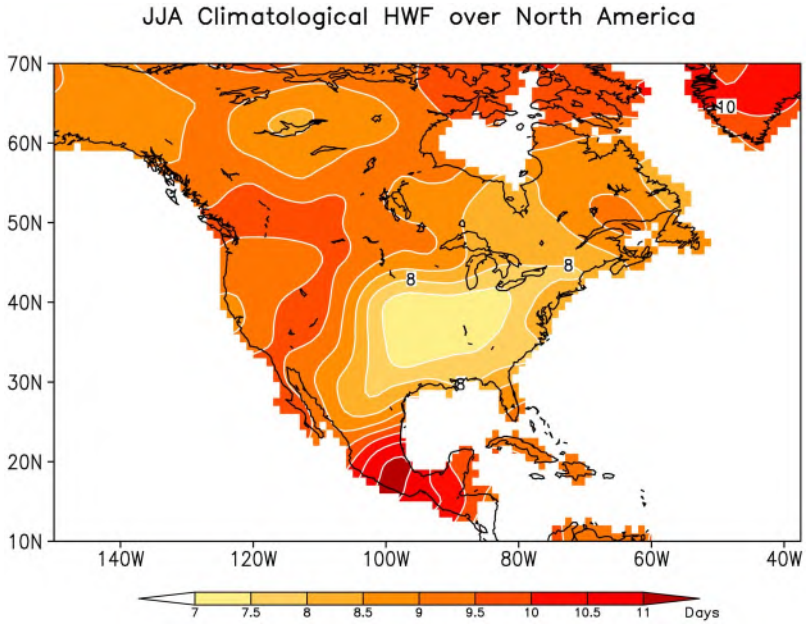

Figure 1. June–August (JJA) climatological heat wave frequency (HWF) over North America (color shadings in units of days).

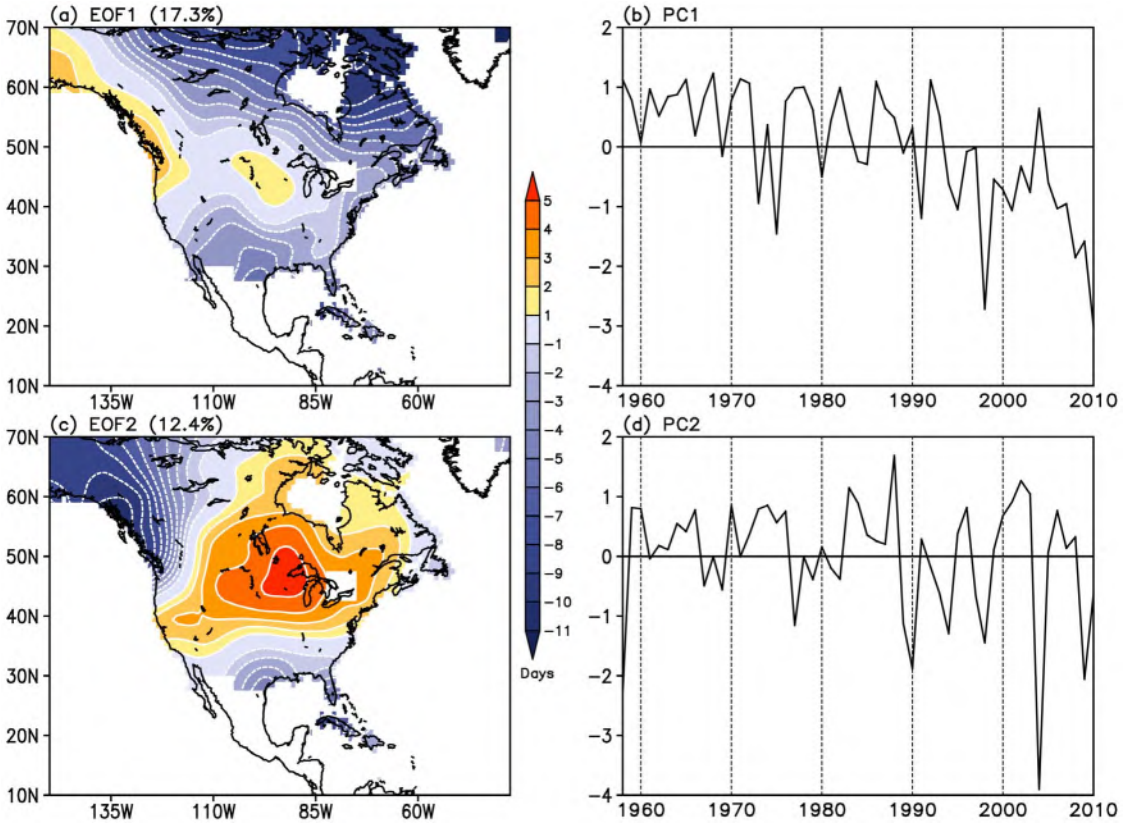

Figure 2. (a) Spatial pattern (color shadings in units of days) and (b) corresponding principal component (PC) of the first empirical orthogonal function (EOF1) mode of the JJA North American HWF. (c and d) Same as Figures 2a and 2b but for the second mode. The numbers in the brackets indicate fractional variance of the EOF modes.

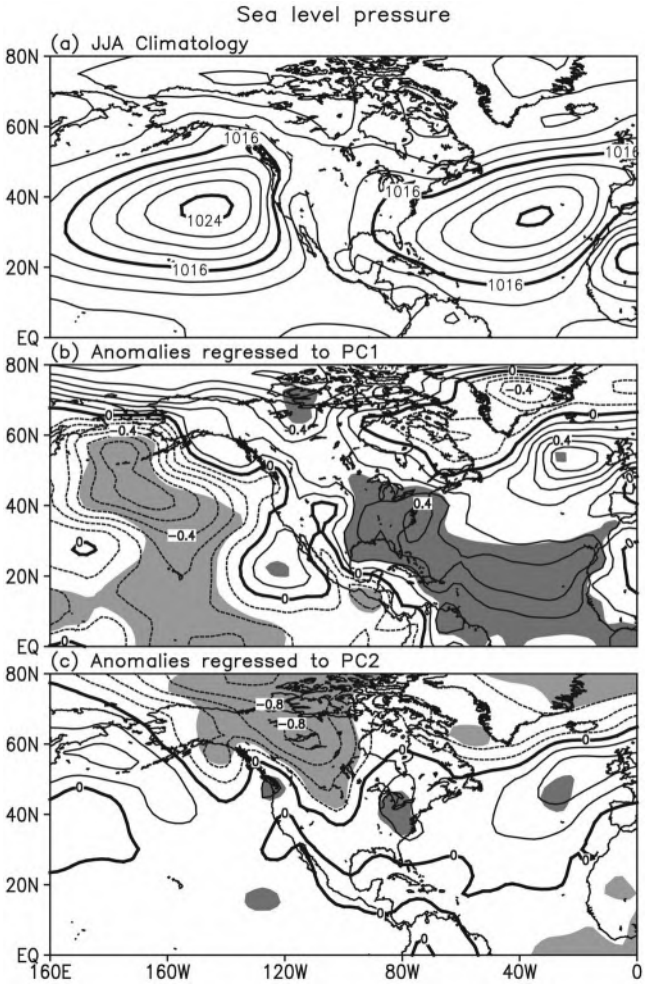

Figure 3. JJA (a) climatology in sea level pressure (contours in units of hPa) and their anomalies regressed to (b) PC1 and (c) PC2. The shaded regions represent anomalies exceeding the 95% confidence level on the basis of a Student's *t* test.

beyond a few days to two weeks [*Lorenz*, 1963]. The predictable variations of heat waves may arise from more slowly varying low boundary conditions, such as oceans and land surface properties [*Namias*, 1959, 1965; *Charney and Shukla*, 1981; *Shukla*, 1998]. Identification of the predictability sources of heat waves may be of central importance for improving their prediction skill. As a matter of fact, *Park and Kung* [1988] examined the antecedent oceanic and atmospheric condition of the principal components of the North American summer temperature field. *Schubert et al.* [2004] found that the most devastating 1930s drought in NA was caused by anomalous tropical sea surface temperature (SST) during that decade. *Lupo et al.* [2008] used the preceding global SST to predict the summer temperature and precipitation for the mid-Mississippi region. Despite the possible intimate linkage among droughts and floods, summer temperature and heat waves, what kind of roles do SST anomalies (SSTAs) play in the heat wave variability?

[5] In addition, there is no universal definition of a heat wave [e.g., *Vincent and Mekis*, 2006; *Peterson et al.*, 2008; *Fischer and Schär*, 2010]. Here, we adopt the criterion proposed by *Fischer and Schär* [2010]. To quantify the strength of heat waves, several indices are proposed; for example, heat wave duration, heat wave amplitude, heat wave number and heat wave frequency (HWF). Owing to high correlations among these indices and the paper length limitation, this study will only focus on the HWF. Its definition will be introduced in section 2.

[6] In this study, we attempt to answer the following questions: What are the basic features of the leading modes of the HWF variability over NA during the past five decades? How are they related to the preceding and simultaneous SSTAs? How do the SSTAs modulate the HWF variations? This paper is structured as follows. Section 2 describes the data sets, model and methodology used in this study. Section 3 introduces the climatological features of the HWF over NA and identifies its two leading modes using an Empirical Orthogonal Function (EOF) analysis. Section 4 presents the large-scale three-dimensional dynamic features associated with the leading modes. In section 5, we examine the SST patterns corresponding to the two leading modes from spring through summer. Numerical experiments are carried out with a simple general circulation model (SGCM) and the possible physical mechanism is discussed in section 6. Section 7 summarizes major findings and some outstanding issues.

2. Data, Model, and Methodology

[7] The primary data used in this study cover the period from 1958 to 2010. Since over East Asia the National Centers for Environmental Prediction (NCEP) reanalysis version 1 (NCEP-1) [*Kalnay et al.*, 1996] data may have systematic errors in the period before 1980 [*Wu et al.*, 2005], we decided to use European Centre for Medium-Range Weather Forecasts (ECMWF) 40-Year Re-Analysis (ERA-40) data [*Uppala et al.*, 2005] for the period 1958–2002 and extend the data from 2003 to 2010 by using NCEP-1 data. To ensure temporal homogeneity, the 2003–2010 NCEP-1 data were adjusted by removing the climatological difference between the ERA-40 and NCEP-1 data sets [*Wang et al.*, 2010].

[8] Other data sets used in this study include: the Global Historical Climatology Network–daily (GHCND) maximum surface air temperature data obtained from the United Kingdom's Hadley Center [*Caesar et al.*, 2006], SST data from the Extended Reconstructed SST Version 2 (ERSST V2) data [*Smith and Reynolds*, 2004], and the precipitation data taken from the monthly global land and ocean precipitation (PREC/LO) data gridded at 2.5° × 2.5° resolution [*Chen et al.*, 2002].

[9] All the numerical experiments are performed using the SGCM as described in the work of *Hall* [2000]. The resolution used here is triangular 31, with 10 equally spaced sigma levels. An important feature of this model is that it uses a time-averaged forcing calculated empirically from observed daily data. In this study, the forcing field is the same as that used in the work of *Lin* [2009] which was derived from the daily data of the NCEP–NCAR reanalysis for the summer season of 1978 to 2007. As shown in several previous studies [e.g., *Hall*, 2000; *Derome et al.*, 2005; *Lin*, 2009], this model is able to reproduce remarkably realistic stationary planetary waves and the broad climatological characteristics of the transients are in general agreement with the observations.

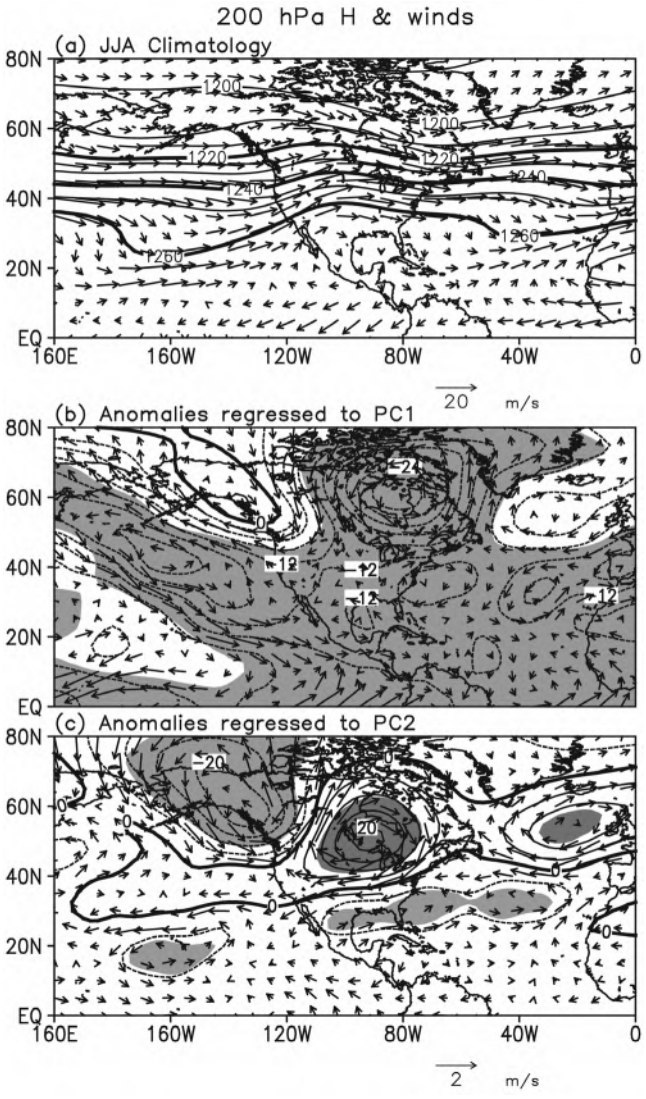

Figure 4. Same as Figure 3 except for 200 hPa geopotential height (H; contours in units of 10 gpm (1 gpm = 0.98 meter)) and winds (vectors; in units of meters per second).

[10] According to the definition by *Fischer and Schär* [2010], a heat wave refers to a spell of at least 6 consecutive days with maximum temperature exceeding the local 90th percentile of the control period (1961–1990). The calculation method is as following: First, the raw daily surface air temperature data is preprocessed by taking a 15 day running mean to remove synoptic fluctuations; Then, the 90th percentile of the control period (1961–1990) is calculated for each calendar day at each grid point from June through August; Finally, the HWF is obtained as the total number of continuous days during which the daily temperature of each is higher than the corresponding 90th percentile value.

3. Climatology and Distinct Leading Modes of HWF Variability

[11] Figure 1 presents the climatology of HWF across NA. High values are observed in western and central Canada, the western United States and Mexico. A prominent feature is a low-value center over the middle and lower reaches of the Mississippi River valley. This center is basically collocated with the high climatological precipitation during summer [e.g., *Huffman et al.*, 1997]. It suggests that the variations in HWF may be linked to precipitation changes. As a matter of fact, the observations and climate models suggest that deficits in soil moisture can lead to more frequent and severe hot summer temperatures, and vice versa [e.g., *Dai et al.*, 1998; *Alexander*, 2010; *Hirschi et al.*, 2010]. The more than normal precipitation often increases the local soil moisture, which in turn favors less frequent heat waves. This may explain why the low HWF center overlaps with the rich precipitation center over the middle and lower reaches of the Mississippi River valley.

[12] Figure 2 shows spatial patterns and the corresponding principal components (PCs) of the two leading modes of the HWF variability. The two leading modes account for 30% of the total HWF variance over entire NA region. According to the rule given by *North et al.* [1982], the two leading modes are statistically distinguished from each other. They are also separable from the rest of the other high modes in terms of sampling error bars (not shown). The first mode shows a general monosign pattern over most of the NA region, except some western coastal areas (Figure 2a). PC1 exhibits a pronounced interdecadal (ID) decreasing trend as well as some interannual variations superposed upon it (Figure 2b). The power spectrum of PC1 exhibits two peaks: a strong ID peak centered around 40 years and a relatively weak interannual (IA) peak around 2 years (not shown). Given the dominance of the ID component, this mode is called the ID mode. Since the negative values of PC1 correspond to more HWF over NA, the PC1 decreasing trend indicates an increasing HWF over most NA region (Figure 2b), which is largely accounted by a sharp transition from a cold to a warm phase in the mid-1980s [e.g., *Trenberth et al.*, 2007].

[13] The most prominent feature of the EOF2 mode is a tripole anomaly pattern with three anomalous centers over the northwestern, central, and southern NA (Figure 2c). The corresponding PC2 shows no trend but significant year-to-year variations (Figure 2d), with an IA spectral peak around 5 years (not shown). In light of this, the EOF2 mode is named as the IA mode. A positive value of PC2 indicates more HWF over central NA and less HWF over northwestern and southern NA, and vice versa. An interesting phenomenon is that the amplitude of PC2 has increased considerably since 1980, indicating that the IA mode becomes more evident in the last three decades.

4. Dynamic Structures of the Leading Modes

[14] Figure 3 shows the anomalous three-dimensional circulations regressed with reference to PC1 and PC2 in order to identify the atmospheric circulation anomalies associated with the two leading HWF patterns. For a strong ID mode (Figure 3b), large areas of negative sea level pressure (SLP) anomalies occupy the North Pacific and expand southeastward, suggesting an intensified Aleutian Low and a weakened Hawaiian High (Figure 3a). Greenland Island and the adjacent areas are also controlled by low SLP anomalies, implying a strengthened Iceland Low. The North Atlantic subtropical high is stronger than normal, associated

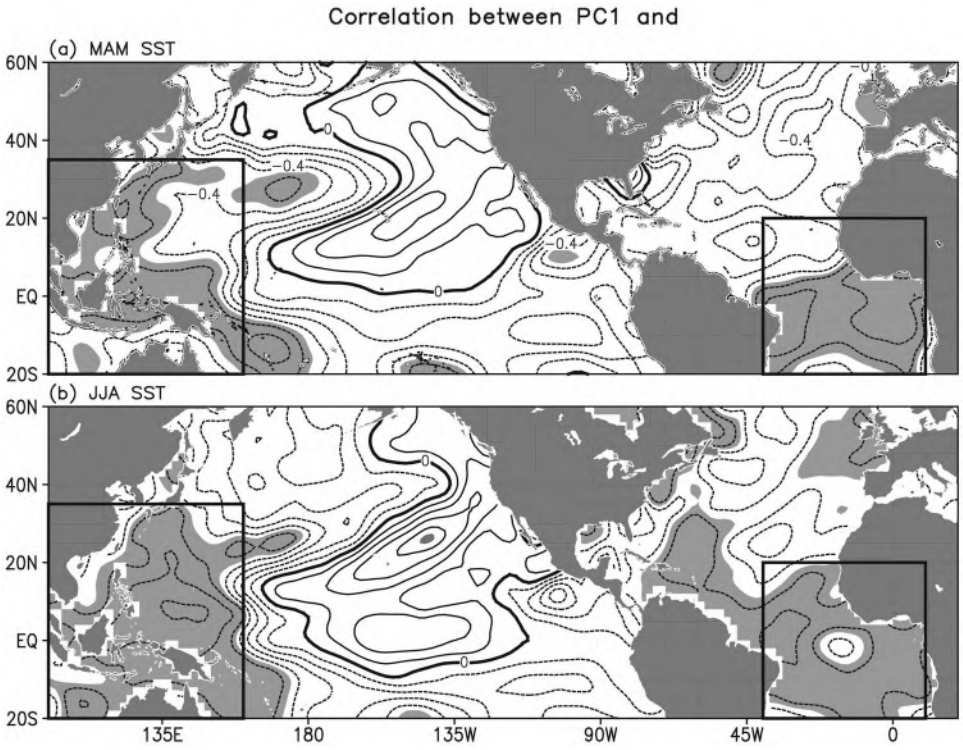

Figure 5. Correlation between PC1 and sea surface temperature (SST) in (a) March-May (MAM) and (b) JJA. The interval of contours is 0.1. The shaded regions represent correlation coefficients exceeding the 95% confidence level on the basis of a Student's *t* test. The oceanic areas within the two boxes are defined as two crucial SST impact regions for the first empirical orthogonal function mode.

with the positive SLP anomalies prevailing over the middle- to low-latitude North Atlantic. Another positive SLP anomaly extends southward from the Arctic Ocean along the western coast of NA (Figure 3b).

[15] For the IA mode (Figure 3c), its positive phase corresponds to negative SLP anomalies in the high latitudes with a center over northwestern Canada, and positive anomalies in the middle latitudes around 40°N. Cold advection over Alaska and the west coast of Canada set up a background of cold surface temperature and reduced HWF in this region as observed in Figure 2c. A positive SLP anomaly belt stretches from the eastern North Atlantic toward the central NA region with a center over eastern NA. The west-east gradient of SLP in central NA with its maximum west of the Great Lakes implies southerly surface wind anomalies which provide a favorable condition for warm weather and enhanced HWF in this area (Figure 2c).

[16] At the upper troposphere, a prominent feature associated with the ID mode is a distinct Rossby wave train propagating from the northwestern Pacific to the north of the NA continent (Figure 4b). Its centers have the same sign and primarily overlap with those near the surface (Figure 3b), indicating a barotropic structure. Since the negative 200 hPa geopotential height (H200) center over northeastern NA is the strongest among the several centers in the Rossby wave train, it is possible that in addition to Rossby wave dissipation there is contribution from other dynamical processes. During a strong ID mode summer, the negative H200 anomalies over northeastern NA tend to deepen the grand NA trough along the eastern coast (Figure 4a), and the associated cyclonic wind anomalies advect more cold air from the Arctic. The positive H200 anomalies stretch southward along the northwestern coast of NA, enhance the climatological ridge and suppress the local cold air activities. Another notable feature is the baroclinic structure over the tropical Atlantic region: the H200 anomalies have an opposite variation tendency with the SLP anomalies (Figures 3b and 4b).

[17] During an anomalous IA mode summer (Figure 4c), the NA region is dominated by a negative H200 anomaly center over the northwest and a positive center which covers most of the continent. The strong negative H200 anomalies over the northwest weaken the climatological ridge (Figure 4a) and may lead this area to expose to cold air from the Arctic. A large positive H200 anomaly center with anticyclonic wind anomalies occupies central-eastern NA, suppressing cold air activities (Figure 4a). In a weak IA mode summer, the situation tends to be opposite.

[18] In general, the two leading modes of the HWF over NA are of considerably different dynamic structures. This implies that their predictability sources may bear substantial differences.

5. SSTAs Associated With the Leading Modes

[19] In order to reveal possible sources of predictability, we search for precursors of the two principal modes in SSTAs during the previous spring. Figure 5a shows the correlation between PC1 and the spring SST. There are two major significant correlation areas. One is located in the tropical Atlantic (TA; 40°W–10°E, 20°S–20°N; see Figure 5a).

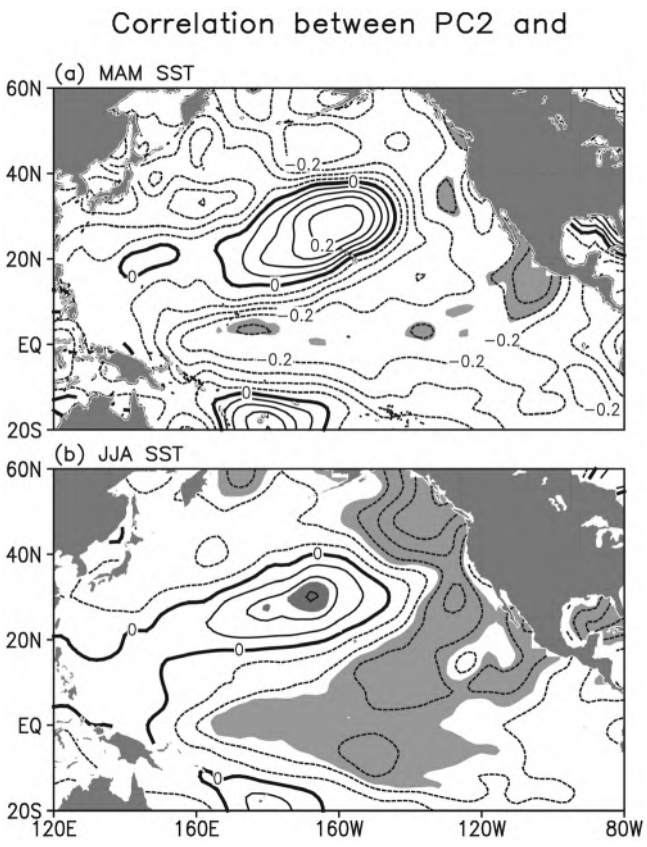

Figure 6. Same as Figure 5 except for PC2.

The other is in the tropical western Pacific (TP; 100°–160°E, 20°S–35°N). If the averaged SSTA in the TA and TP regions are defined as two SSTA indices, the correlation coefficients between PC1 and the two SSTA indices reach –0.74 and −0.68, respectively, exceeding the 95% confidence level on the basis of a Student's *t* test. These significant correlations can persist through the following summer, which makes them possible predictability sources for the ID mode (Figure 5b).

[20] For the IA mode, it exhibits an enhanced linkage with the SSTA in the equatorial eastern Pacific from the prior spring through the following summer (Figure 6). In preceding spring, the correlation between PC2 and SSTA in eastern Pacific is rather weak (Figure 6a), whereas it becomes significant in following summer (Figure 6b). This indicates that the development of ENSO events might provide a major predictability source for the IA mode. The influence of the tropical diabatic forcing associated with ENSO extends to NA through atmospheric teleconnections (i.e., the Pacific-North America (PNA) pattern), which has been well documented [e.g., *Horel and Wallace*, 1981; *Ropelewski and Halpert*, 1986; *Hurrell*, 1996; *Lau*, 1997; *Lin and Wu*, 2011; *Wu et al.*, 2011]. In the following, we would focus on the formation of the atmospheric general circulation anomalies corresponding to the ID mode.

[21] SST variability can influence atmospheric circulation through different processes [e.g., *Charney and Shukla*, 1981; *Shukla*, 1998; *Wu et al.*, 2009a]. Changes in precipitation and atmospheric diabatic heating associated with SSTAs, for example, provide an important forcing mechanism for the atmospheric circulation. To illustrate the relationship between SST variability in the TA and TP regions and precipitation, Figure 7 presents the rainfall anomalies regressed against the TA and TP SSTA index. Regions with anomalies that are 5% statistically significant according to a Student's *t* test are shaded. It can be clearly seen from Figure 7 that the warm SSTA is usually associated with enhanced precipitation over the local region. For a warm TA SSTA, an intensified rainfall belt can be discerned within the region (80°–10°W, 10°S–10°N), with three anomaly centers located in the TA oceanic area, the lower reaches of the Amazon River, and Panama City. For a warm TP SSTA, a rich precipitation anomaly center covers the oceanic region (130°–160°E, 25°–40°N) southeast of the Japan islands. The situations during the cold SSTA conditions tend to be opposite.

[22] To evaluate the contributions of these possible predictability sources to the atmospheric general circulation, we calculated the composite difference of H200 and SLP between the cold and warm TA, TP summers (Figures 8 and 9). Note that a warm TA or TP summer refers to the corresponding SSTA index above 1 standard deviation, where a cold TA or TP summer below −1 standard deviation. When a cold or warm SSTA emerges in the TA region, the circulation anomalies are of a baroclinic structure over the TA region expanding toward the middle latitudes in both hemispheres (Figure 8). The upper level is controlled by a zonally elongated negative H200 anomaly and the surface by significantly positive SLP. This indicates that the SLP over the TA region associated with a negative TA SSTA is stronger than that with a positive TA SSTA, and the H200 variation

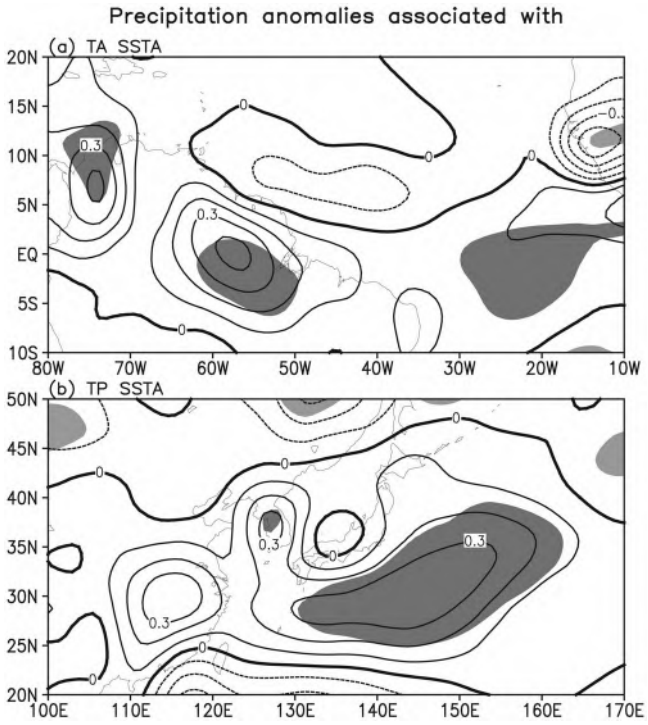

Figure 7. Observed precipitation anomalies (contours in units of millimeters per day) regressed to the mean SSTA within the boxes in the (a) tropical Atlantic (TA) and (b) tropical western Pacific (TP) as shown in Figure 5. The shaded regions exceed the 95% confidence level on the basis of a Student's *t* test.

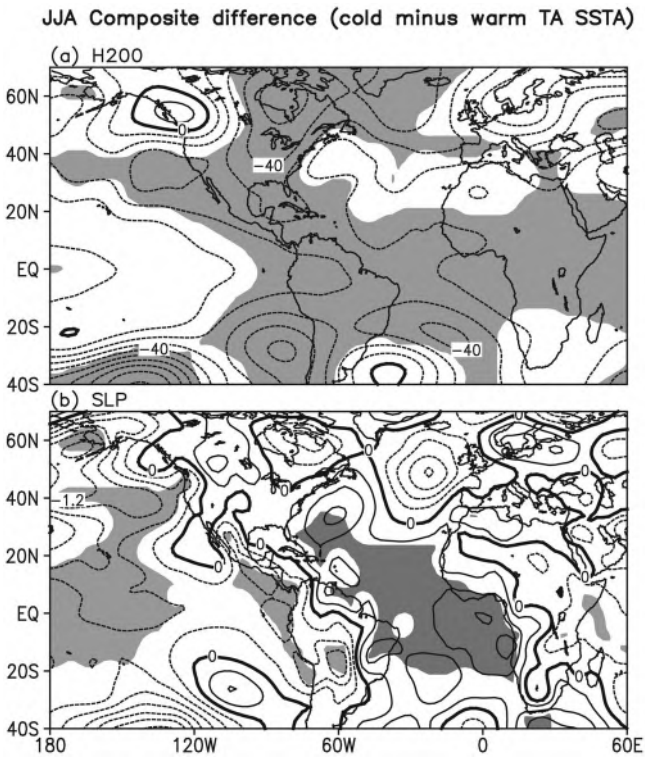

Figure 8. Composite differences between the cold and warm TA SSTA summers (cold minus warm) for (a) 200 hPa H (H200) and (b) sea level pressure (SLP). A cold (warm) TA SSTA summer refers to the JJA mean SSTA in the TA region greater than (less than) 1 (−1) standard deviation. The shaded areas exceed the 95% confidence level on the basis of a Student's *t* test.

tendency is just opposite to the SLP. Such a baroclinic structure can be interpreted as tropical atmospheric responses to the TA diabatic heating [e.g., *Kucharski et al.*, 2009; *Wu et al.*, 2012]. Another evidence supporting the notion that the exhibited atmospheric anomalies are responses to the anomalous TA diabatic heating rather than vice versa is that the circulation differences are quite symmetric about the equator. This structure resembles an equatorial Rossby wave response to a tropical heating located near TA [*Matsuno*, 1966; *Gill*, 1980].

[23] For the TP SSTA (Figure 9), the circulation anomaly north of 40°N is of an equivalent barotropic structure. Significantly negative anomalies in both H200 and SLP prevail over the region from the North Pacific to eastern NA. This barotropic structure reflects that the anomaly is an extratropical response to a remote forcing. On the other hand, the circulation anomaly bears a baroclinic structure over the oceanic areas southeast of the Japan islands where the anomalous rainfall is located (Figure 7b). To summarize, the SSTA in the TA and TP regions may be two predictability sources of the ID mode, whereas developing phases of ENSO events probably signify a precursory condition for the IA mode.

6. Numerical Experiments

[24] To support the above hypothesis, we conducted numerical experiments with the SGCM model. To mimic the diabatic heating effects of the SSTA in the TA and TP regions, we imposed two heating anomaly sources, each having an elliptical squared cosine distribution in latitude and longitude. On the basis of the previous work by *Hoskins and Karoly* [1981], the vertically integrated heating rate imposed here is 1.25 K/day, which is approximately the latent heating rate release given by an extra 5 mm precipitation per day. The vertical heating profile peaks at around 300 hPa [*Lin*, 2009; *Wu et al.*, 2009b, 2012]. Two perturbed experiments were integrated for 3700 days, one with an anomalous cooling and the other with an anomalous heating. Daily output of the last 3600 days is used to calculate the model climate under each forcing condition. Note that the result is not sensitive to the selection of initial condition, since the analysis is conducted for the period after the climate equilibrium is reached.

[25] It can be clearly seen from Figure 10 that under the TA SSTA forcing (cooling minus warming), the 150 hPa geopotential height (H150) difference resembles an equatorial Rossby wave response with a pair of cyclonic circulations straddling the equator, which is similar to the observation (Figure 8). The vertical structure of the response is baroclinic with an opposite variation tendency between SLP and H150 (not shown). Under the TP SSTA forcing, Figure 11 indicates that the atmospheric response takes the form of an eastward propagating Rossby wave train. Over the NA continent, most regions are controlled by negative H150 anomalies, except some western coastal areas. The coeffects of the above two response patterns tend to strengthen the atmosphere general circulation anomalies over the NA continent, namely, the negative H150 anomalies over most NA regions and the positive H150 anomalies over the western coastal areas. This may at least partly explain why the observed H200 anomaly center over the NA continent is the strongest one among the several centers in the Rossby wave train (Figure 4b).

[26] The consistency between the results from the numerical experiments and from the previous observational analysis indicates that the diabatic forcing associated with the anomalous SST in the TA and TP regions can contribute to the circulation anomalies associated with the ID mode of HWF over NA. For the IA mode, the circulation anomalies basically result from the development of ENSO. Since the physical linkage between the atmospheric anomalies and ENSO has been relatively well recognized, in this study we will not repeat the relevant numerical experiments.

7. Conclusion and Discussion

[27] Understanding their related large-scale circulations and preceding low boundary conditions may be of central importance for seasonal prediction of climate extremes such as heat waves [e.g., *Easterling et al.*, 2000; *Wu et al.*, 2010; *Birk et al.*, 2010; *Lin and Wu*, 2011; *Wu et al.*, 2011]. In this study, we find that the HWF over NA is dominated by two distinct leading modes: the ID and IA modes. The ID mode primarily depicts a HWF increasing pattern over most of the NA continent except some western coastal areas. The IA mode resembles a tripole HWF anomaly pattern with three centers over the northwestern, central, and southern NA. The potential predictability sources for the two distinct modes are also examined. The ID mode is intimately connected with the SSTA in the TA and TP regions in the prior spring. The

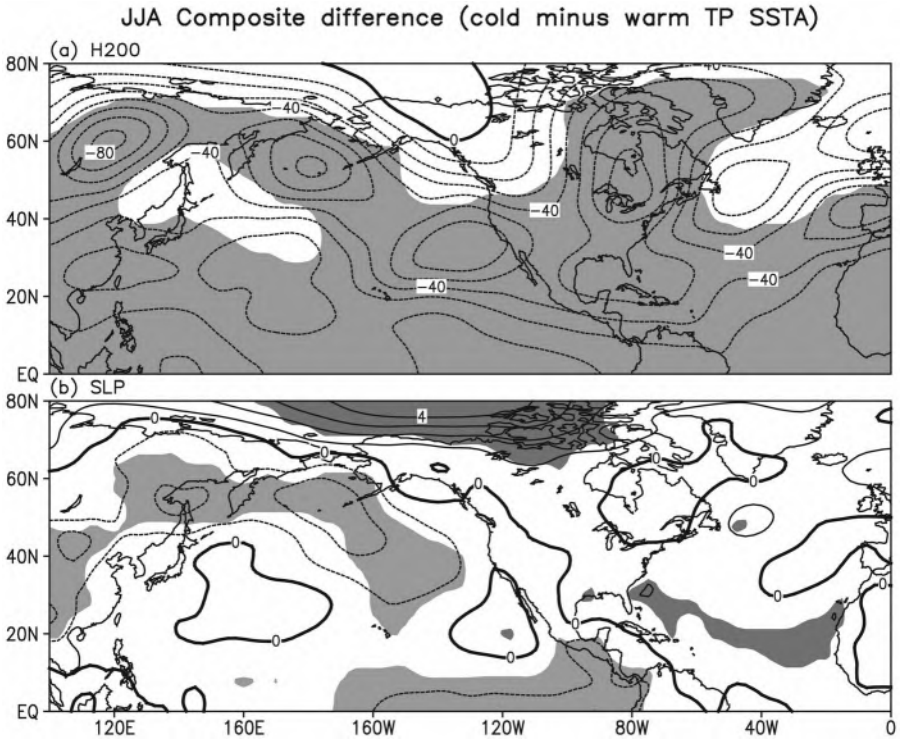

Figure 9. Same as Figure 8 except for the TP SSTA.

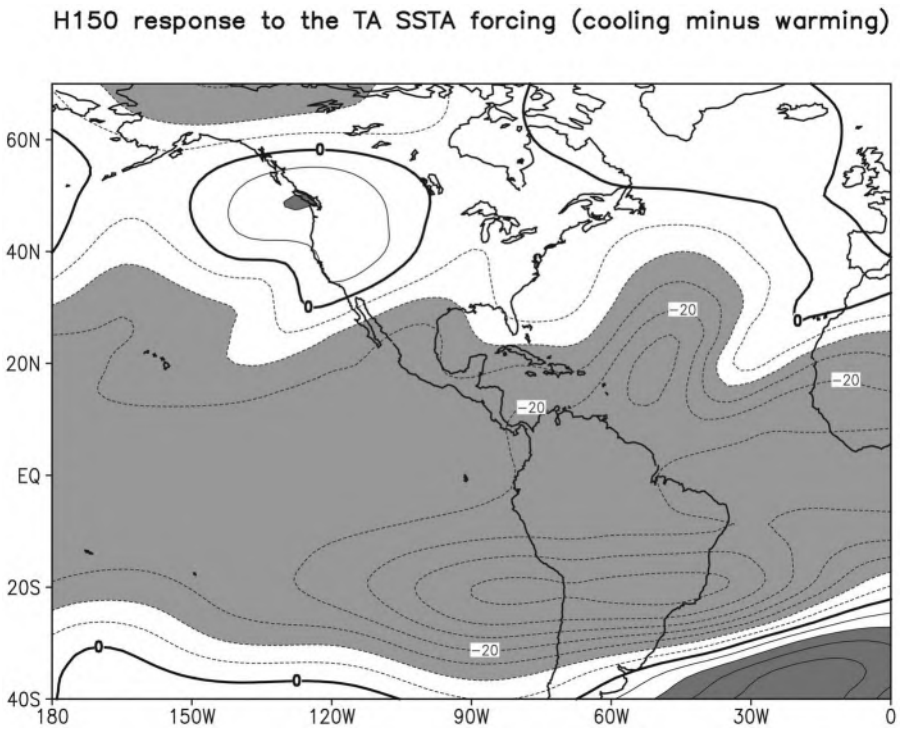

Figure 10. The 150 hPa H (H150) responses (contours in units of gpm; 1 gpm = 0.98 meter) in the simple general circulation model (SGCM) regarding a cold and warm TA SSTA forcing in summer (cold minus warm). The H150 anomalies in the dark shaded areas are greater than 10 gpm, while those in the light shaded areas less than −10 gpm.

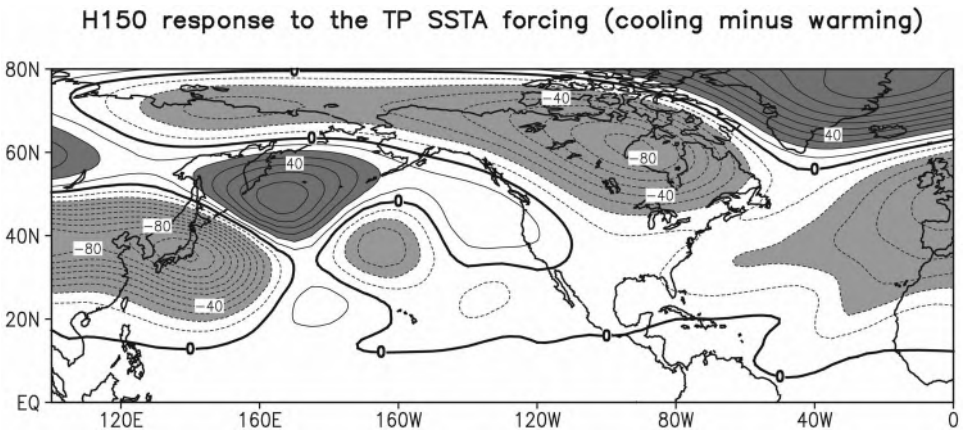

Figure 11. Same as Figure 10 except for the TP SSTA forcing.

IA mode may be influenced not necessarily by the phase of ENSO, but the change of phase in ENSO. These low boundary anomalies can persist from spring through summer.

[28] The possible physical mechanism is also investigated with the SGCM. For the ID mode, the tropical Atlantic SSTA can induce a Gill-type response which extends over NA, while the northwestern Pacific SSTA excites a Rossby wave train propagating eastward toward NA. These two flow patterns contribute to the large-scale circulation anomalies associated with the ID mode. For the IA mode, its circulation anomalies basically results from the teleconnection pattern excited by ENSO.

[29] How could the large-scale circulation anomalies influence the HWF? *Namias* [1982, 1983] found that a protracted heat wave during summer was a manifestation of an abnormal form of the general circulation. *Hoskins et al.* [1983] suggested a theory of positive feedback between the synoptic eddies and the seasonal mean flow. On the basis of the results in this study and those obtained by *Hirschi et al.* [2010] and *Alexander* [2010], the physical processes between the circulation anomalies and HWF may be summarized as following. The SSTAs associated with the ID and IA modes trigger the corresponding teleconnection patterns propagating toward NA and excite high- or low-pressure anomalies over the local region. The subsidence associated with high-pressure anomalies warms and dries the boundary layer, inhibiting cloud formation. The resulting surface radiative heating further warms the surface. For the low-pressure anomalies, the situation is just opposite. Through such processes, these SSTAs can exert profound influences to the HWF variability over NA.

[30] Besides the above SSTAs, the two distinct HWF modes may have other predictability sources (snow cover, sea ice concentration and soil moisture, etc.). Figure 4 shows that for both the ID mode and IA mode, there is much larger variability in the high latitudes than the tropical region. This implies that the high-latitude forcings may also play some roles. Owing to data limitation, their roles are still not clear. Therefore, one of the biggest problems in performing analysis of extreme weather and climate events such as heat waves may be the lack of access to high-quality, long-term low boundary data [*Easterling et al.*, 2000]. For example, snow cover data is available only from 1968 [e.g., *Lin and Wu*, 2011], and there are few soil moisture gauge stations over NA. If more accurate low boundary data is available, we might understand more in-depth processes governing these extreme events.

[31] **Acknowledgments.** Zhiwei Wu is supported by the Sustainable Agriculture Environment Systems research initiative of Agriculture and Afri-Food Canada through the Natural Sciences and Engineering Research Council of Canada Fellowship Program and the National Basic Research Program 973 (grant 2010CB950400).

References

Alexander, L. (2010), Extreme heat rooted in dry soils, *Nat. Geosci.*, *3*, 1–2, doi:10.1038/ngeo1045.

Birk, K., A. R. Lupo, P. E. Guinan, and C. E. Barbieri (2010), The interannual variability of midwestern temperatures and precipitation as related to the ENSO and PDO, *Atmosfera*, *23*, 95–128.

Caesar, J., L. Alexander, and R. Vose (2006), Large-scale changes in observed daily maximum and minimum temperatures: Creation and analysis of a new gridded data set, *J. Geophys. Res.*, *111*, D05101, doi:10.1029/2005JD006280.

Charney, J. G., and J. Shukla (1981), Predictability of monsoons, in *Monsoon Dynamics*, edited by J. Lighthill and R. P. Pearce, pp. 99–109, Cambridge Univ. Press, New York.

Chen, M., P. Xie, J. E. Janowiak, and P. A. Arkin (2002), Global land precipitation: A 50-yr monthly analysis based on gauge observations, *J. Hydrometeorol.*, *3*, 249–266, doi:10.1175/1525-7541(2002)003<0249:GLPAYM>2.0.CO;2.

Dai, A. G., K. E. Trenberth, and T. R. Karl (1998), Global variations in droughts and wet spells: 1900−1995, *Geophys. Res. Lett.*, *25*, 3367–3370, doi:10.1029/98GL52511.

Derome, J., H. Lin, and G. Brunet (2005), Seasonal forecasting with a simple general circulation model, *J. Clim.*, *18*, 597–609, doi:10.1175/JCLI-3289.1.

Ding, Y. H., G. Y. Ren, Z. C. Zhao, Y. Xu, Y. Luo, Q. P. Li, and J. Zhang (2007), Detection, causes and projection of climate change over China: An overview of recent progresses, *Adv. Atmos. Sci.*, *24*, 954–971, doi:10.1007/s00376-007-0954-4.

Easterling, D. R., J. L. Evans, P. Y. Groisman, K. E. Kunkel, and P. Ambenje (2000), Observed variability and trends in extreme climate events: A brief review, *Bull. Am. Meteorol. Soc.*, *81*, 417–425, doi:10.1175/1520-0477(2000)081<0417:OVATIE>2.3.CO;2.

Fischer, E. M., and C. Schär (2010), Consistent geographical patterns of changes in high-impact European heatwaves, *Nat. Geosci.*, *3*, 398–403, doi:10.1038/ngeo866.

Garcia-Herrera, R., J. Diaz, R. M. Trigo, J. Luterbacher, and E. M. Fischer (2010), A review of the European summer heat wave of 2003, *Crit. Rev. Environ. Sci. Technol.*, *40*, 267–306, doi:10.1080/10643380802238137.

Gill, A. E. (1980), Some simple solutions for heat-induced tropical circulations, *Q. J. R. Meteorol. Soc.*, *106*, 447–462, doi:10.1002/qj.49710644905.

Hall, N. M. J. (2000), A simple GCM based on dry dynamics and constant forcing, *J. Atmos. Sci.*, *57*, 1557–1572, doi:10.1175/1520-0469(2000)057<1557:ASGBOD>2.0.CO;2.

Hirschi, M., S. I. Seneviratne, V. Alexandrov, F. Boberg, C. Boroneant, O. B. Christensen, H. Formayer, B. Orlowsky, and P. Stepanek (2010),

Observational evidence for soil-moisture impact on hot extremes in southeastern Europe, *Nat. Geosci.*, *3*, 17–21, doi:10.1038/ngeo1032.

Horel, J. D., and J. M. Wallace (1981), Planetary-scale atmospheric phenomena associated with the Southern Oscillation, *Mon. Weather Rev.*, *109*, 813–829, doi:10.1175/1520-0493(1981)109<0813:PSAPAW>2.0.CO;2.

Hoskins, B. J., and D. J. Karoly (1981), The steady linear response of a spherical atmosphere to thermal and orographic forcing, *J. Atmos. Sci.*, *38*, 1179–1196, doi:10.1175/1520-0469(1981)038<1179:TSLROA>2.0.CO;2.

Hoskins, B. J., I. N. James, and G. H. White (1983), The shape, propagation, and mean-flow interaction of large-scale weather systems, *J. Atmos. Sci.*, *40*, 1595–1612, doi:10.1175/1520-0469(1983)040<1595:TSPAMF>2.0.CO;2.

Huffman, G. J., R. F. Adler, P. Arkin, A. Chang, R. Ferraro, A. Gruber, J. Janowiak, A. McNab, B. Rudolf, and U. Schneider (1997), The Global Precipitation Climatology Project (GPCP) combined precipitation dataset, *Bull. Am. Meteorol. Soc.*, *78*, 5–20, doi:10.1175/1520-0477(1997)078<0005:TGPCPG>2.0.CO;2.

Hurrell, J. W. (1996), Influence of variations in extratropical wintertime teleconnections on Northern Hemisphere temperature, *Geophys. Res. Lett.*, *23*, 665–668, doi:10.1029/96GL00459.

Kalnay, E., et al. (1996), The NCEP/NCAR 40-year reanalysis project, *Bull. Am. Meteorol. Soc.*, *77*, 437–471, doi:10.1175/1520-0477(1996)077<0437:TNYRP>2.0.CO;2.

Karl, T. R., and D. R. Easterling (1999), Climate extremes: Selected review and future research directions, *Clim. Change*, *42*, 309–325, doi:10.1023/A:1005436904097.

Karl, T. R., and K. E. Trenberth (2003), Modern global climate change, *Science*, *302*, 1719–1723, doi:10.1126/science.1090228.

Kucharski, F., A. Bracco, J. H. Yoo, A. Tompkins, L. Feudale, P. Ruti, and A. Dell'Aquila (2009), A Gill-Matsun-type mechanism explains the tropical Atlantic influence on African and Indian monsoon rainfall, *Q. J. R. Meteorol. Soc.*, *135*, 569–579, doi:10.1002/qj.406.

Lau, N.-C. (1997), Interactions between global SST anomalies and the midlatitude atmospheric circulation, *Bull. Am. Meteorol. Soc.*, *78*, 21–33, doi:10.1175/1520-0477(1997)078<0021:IBGSAA>2.0.CO;2.

Lin, H. (2009), Global extratropical response to diabatic heating variability of the Asian summer monsoon, *J. Atmos. Sci.*, *66*, 2697–2713, doi:10.1175/2009JAS3008.1.

Lin, H., and Z. Wu (2011), Contribution of the autumn Tibetan Plateau snow cover to seasonal prediction of North American winter temperature, *J. Clim.*, *24*, 2801–2813, doi:10.1175/2010JCLI3889.1.

Lorenz, E. N. (1963), Deterministic nonperiodic flow, *J. Atmos. Sci.*, *20*, 130–141, doi:10.1175/1520-0469(1963)020<0130:DNF>2.0.CO;2.

Lupo, A. R., E. P. Kelsey, D. K. Weitlich, N. A. Davis, and P. S. Market (2008), Using the monthly classification of global SSTs and 500 hPa height anomalies to predict temperature and precipitation regimes one to two seasons in advance for the mid-Mississippi region, *Natl. Weather Dig.*, *32*, 1–23.

Matsuno, T. (1966), Quasi-geostrophic motions in the equatorial area, *J. Meteorol. Soc. Jpn.*, *44*, 25–43.

Meehl, G. A., and C. Tebaldi (2004), More intense, more frequent, and longer lasting heat waves in the 21st century, *Science*, *305*, 994–997, doi:10.1126/science.1098704.

Meehl, G. A., W. M. Washington, C. M. Ammann, J. M. Arblaster, T. M. L. Wigley, and C. Tebaldi (2004), Combinations of natural and anthropogenic forcings in twentieth-century climate, *J. Clim.*, *17*, 3721–3727, doi:10.1175/1520-0442(2004)017<3721:CONAAF>2.0.CO;2.

Namias, J. (1959), Recent seasonal interaction between North Pacific waters and the overlying atmospheric circulation, *J. Geophys. Res.*, *64*, 631–646, doi:10.1029/JZ064i006p00631.

Namias, J. (1965), Macroscopic association between monthly mean sea-surface temperature and overlying winds, *J. Geophys. Res.*, *70*, 2307–2318, doi:10.1029/JZ070i010p02307.

Namias, J. (1982), Anatomy of great plains protracted heat waves (especially the 1980 U.S. summer drought), *Mon. Weather Rev.*, *110*, 824–838, doi:10.1175/1520-0493(1982)110<0824:AOGPPH>2.0.CO;2.

Namias, J. (1983), Some causes of the United States drought, *J. Clim. Appl. Meteorol.*, *22*, 30–39, doi:10.1175/1520-0450(1983)022<0030:SCOUSD>2.0.CO;2.

North, G. R., T. L. Bell, R. F. Cahalan, and F. J. Moeng (1982), Sampling errors in the estimation of empirical orthogonal functions, *Mon. Weather Rev.*, *110*, 699–706, doi:10.1175/1520-0493(1982)110<0699:SEITEO>2.0.CO;2.

Park, C.-K., and E. C. Kung (1988), Principal components of the North American summer temperature field and the antecedent oceanic and atmospheric condition, *J. Meteorol. Soc. Jpn.*, *66*, 677–690.

Peterson, T. C., X. Zhang, M. Brunet-India, and J. L. Vázquez-Aguirre (2008), Changes in North American extremes derived from daily weather data, *J. Geophys. Res.*, *113*, D07113, doi:10.1029/2007JD009453.

Ropelewski, C. F., and M. S. Halpert (1986), North American precipitation and temperature patterns associated with the El Niño/Southern Oscillation (ENSO), *Mon. Weather Rev.*, *114*, 2352–2362, doi:10.1175/1520-0493(1986)114<2352:NAPATP>2.0.CO;2.

Schubert, S. D., M. J. Suarez, P. J. Pegion, R. D. Koster, and J. T. Bacmeister (2004), On the cause of the 1930s dust bowl, *Science*, *303*, 1855–1859, doi:10.1126/science.1095048.

Shukla, J. (1998), Predictability in the midst of chaos: A scientific basis for climate forecasting, *Science*, *282*, 728–731, doi:10.1126/science.282.5389.728.

Smith, T. M., and R. W. Reynolds (2004), Improved extended reconstruction of SST (1854−1997), *J. Clim.*, *17*, 2466–2477, doi:10.1175/1520-0442(2004)017<2466:IEROS>2.0.CO;2.

Trenberth, K. E., et al. (2007), Observations: Surface and Atmospheric Climate Change, in *Climate Change 2007: The Physical Science Basis, Contribution of Working Group 1 to the Fourth Assessment Report of the Intergovernmental Panel on Climate Change*, edited by S. Solomon et al., pp. 235–336, Cambridge Univ. Press, New York.

Uppala, S. M., et al. (2005), The ERA-40 re-analysis, *Q. J. R. Meteorol. Soc.*, *131*, 2961–3012, doi:10.1256/qj.04.176.

Vincent, L. A., and E. Mekis (2006), Changes in daily and extreme temperature and precipitation indices for Canada over the twentieth century, *Atmos. Ocean*, *44*, 177–193, doi:10.3137/ao.440205.

Wang, B., and Q. Ding (2006), Changes in global monsoon precipitation over the past 56 years, *Geophys. Res. Lett.*, *33*, L06711, doi:10.1029/2005GL025347.

Wang, B., Z. Wu, J. Liu, C.-P. Chang, J. Li, and T.-J. Zhou (2010), Another look at climate variations of the East Asian winter monsoon: Northern and southern modes, *J. Clim.*, *23*, 1495–1512, doi:10.1175/2009JCLI3243.1.

Wu, R., J. L. Kinter III, and B. P. Kirtman (2005), Discrepancy of interdecadal changes in the Asian region between the NCEP-NCAR reanalysis and observations, *J. Clim.*, *18*, 3048–3067, doi:10.1175/JCLI3465.1.

Wu, Z., J. Li, B. Wang, and X. Liu (2009a), Can the Southern Hemisphere annular mode affect China winter monsoon?, *J. Geophys. Res.*, *114*, D11107, doi:10.1029/2008JD011501.

Wu, Z., B. Wang, J. Li, and F.-F. Jin (2009b), An empirical seasonal prediction model of the East Asian summer monsoon using ENSO and NAO, *J. Geophys. Res.*, *114*, D18120, doi:10.1029/2009JD011733.

Wu, Z., J. Li, Z. Jiang, and J. He (2010), Predictable climate dynamics of abnormal East Asian winter monsoon: Once-in-a-century snowstorms in 2007/2008 winter, *Clim. Dyn.*, *37*, 1661–1669, doi:10.1007/s00382-010-0938-4.

Wu, Z., H. Lin, and T. Brien (2011), Seasonal prediction of air temperature associated with the growing season start of warm-season crops across Canada, *J. Appl. Meteorol. Climatol.*, *50*, 1637–1649, doi:10.1175/2011JAMC2676.1.

Wu, Z., J. Li, Z. Jiang, J. He, and X. Zhu (2012), Possible effects of the North Atlantic Oscillation on the strengthening relationship between the East Asian summer monsoon and ENSO, *Int. J. Climatol.*, doi:10.1002/joc.2309, in press.

Z. Jiang and T. Ma, Key Laboratory of Meteorological Disaster of Ministry of Education, University of Information Science and Technology, Nanjing 210044, China.

J. Li, State Key Laboratory of Numerical Modeling for Atmospheric Sciences and Geophysical Fluid Dynamics, Institute of Atmospheric Physics, Chinese Academy of Sciences, Beijing 100029, China.

H. Lin and Z. Wu, Meteorological Research Division, Environment Canada, 2121 Route Transcanadienne, Dorval, QC H9P 1J3, Canada. (zhiwei.wu@ec.gc.ca)